TOWARDS AUTOMATED LIDAR BORESIGHT SELF-CALIBRATION

J. Skaloud [a, *], P. Schaer [a]

[a] TOPO Lab, Ecole Polytechnique Fédérale de Lausanne (EPFL), Station 18, 1015 Lausanne, Switzerland

KEY WORDS: airborne laser scanning, LiDAR, boresight, calibration, classification, roof detection

ABSTRACT:

This paper focuses on practical aspects when performing boresight calibration in airborne laser scanning using rigorous methodology implemented in LIBOR software. LIBOR technique, introduced by (Skaloud and Lichti, 2006), is based on expressing the boresight calibration parameters within the direct-georeferencing equation separately for each target point and conditioning a group of points to lie on a common planar surface. Although there is no need for a priori information about the plane parameters as these are part of the unknowns, good estimation requires implication of various planar features that differ in slope and orientation. Such conditions are typically fulfilled in residential-urban areas where the presence of planes in form of roof-tops is abundant. These are identified by grouping points belonging to the same surface into a distinct class separately for each flight line and finding class-correspondences among the flight lines. We present an automated approach for this selection process that stems from intrinsic geometry of curved surfaces. This classification is followed by additional fine-filtering for returns from features as chimneys, antennas etc. The presented discussion focuses on practical examples with data from continuously-rotating and oscillating-mirror systems. These findings show that good automated point selection is possible and acts as a pre-requisite to robust estimates of all boresight angles with accuracy that is several times superior to the system noise level.

1. INTRODUCTION

In contrary to relatively well developed approaches to boresight estimation between an Inertial Measurement Unit (IMU) and frame/line-based imagery (Cramer and Stallmann, 2002; Kruck, 2001; Skaloud and Schaer, 2003) the existing procedures for the LiDAR-IMU misalignment, while functional, are recognized as being suboptimal and much research is devoted to their improvement. The adopted approaches are usually based either on physical boundaries or cross-sections (Schenk, 2001), DTM gradients (Burman, 2000) or mimic the photogrammetric calibration approach via signalized or intensity-deduced targets points (Morin, 2002). The drawback of these methods is the lack (or simplification) of assurance measures, correlation with the unknown terrain shape or limits imposed by laser pointing accuracy and uncertainty due to beam-width. Not long ago, a more rigorous class of calibration procedures started to emerge (Filin, 2003; Friess, 2006; Skaloud and Lichti, 2006). These types of approaches model all systematic errors directly in the measurement domain and condition groups of points to reside on a common surface of known form. This alleviates the problem of LiDAR beam-pointing uncertainty experienced in photogrammetry-like approaches while preserving the correct formulation of the observation equation for each point separately. It was also demonstrated that estimating the calibration parameters together with those of surfaces does not compromise the estimate of the boresight (Skaloud and Lichti, 2006) and the self-calibrating scheme is indeed possible. We will exploit this approach further with the aim of achieving its complete automation when selecting and classifying the needed planar features.

The organization of the paper is as follows. After recalling the functional model for the recovery of calibration parameters we propose an algorithm for automated detection and extraction of the planar section of the rooftops. After that we present a synthesis of our practical experience when applying this approach to airborne scanners of different type (i.e. oscillating or continuously rotating mirror) and providers (e.g. Optech, Leica, Riegl).

2. ESTIMATION MODEL

Following (Skaloud and Lichti, 2006) the functional model is based on conditioning the georeferenced LiDAR target points to lie on surfaces of known form, particularly planes. The plane coefficients are estimated together with the calibration parameters. The *a-priori* unknowns of a plane *j* are represented as $\vec{s}_j = \begin{bmatrix} s_{1_j} & s_{2_j} & s_{3_j} & s_{4_j} \end{bmatrix}^T$ and the desired form of the condition used for the parameter estimation reads:

$$\left\langle \vec{s}_j, \begin{bmatrix} \begin{bmatrix} X_i \\ Y_i \\ Z_i \end{bmatrix} + R^m_{b_i} \left(\begin{bmatrix} u_i \\ v_i \\ w_i \end{bmatrix} + U_i \begin{bmatrix} \alpha \\ \beta \\ \gamma \end{bmatrix} + \vec{a} \right) \\ 1 \end{bmatrix} \right\rangle = 0 \qquad (1)$$

where, $\vec{g} = \begin{bmatrix} X & Y & Z \end{bmatrix}^T$ are the coordinates of IMU-centre in the mapping frame at time *i*, $R^m_{b_i} = f(r, p, y)$ is the orientation matrix from the IMU body frame (*b*) to the mapping frame parameterized by roll (*r*), pitch (*p*) and yaw (*y*) observations at time *i*, $\vec{a}$ is the lever-arm offset between the IMU and LiDAR measurement centers expressed in the IMU body frame, α, β and γ are the unknown boresight angles and *U* is the skew-symmetric matrix of LiDAR vector $\vec{u}$ defined by means of the mounting orientation matrix (T^{b*}_s) as well as encoder (θ) and range (ρ) measurements and as:

$$\vec{u} = \begin{bmatrix} u & v & w \end{bmatrix}^T \equiv T^{b*}_s \begin{bmatrix} (\rho + \Delta\rho)\sin\theta \\ 0 \\ (\rho + \Delta\rho)\cos\theta \end{bmatrix} \qquad (2)$$

* Corresponding author. Tel: +41 21 693 27 55 / Fax: +41 21 693 57 40 / email: jan.skaloud@epfl.ch

Other system-related calibration parameters can be expressed in the Eq. (2), as it is the case for a constant range finder offset $\Delta\rho$. The Eq. (1) contains two sets of unknowns, first related to the boresight and systematic laser errors and second related to plane coefficients. The combined (or Gauss-Helmert) adjustment model is used after the linearization in estimating the corrections of the parameter sets $\hat{\delta}_1, \hat{\delta}_2$ from a relation:

$$\begin{bmatrix} A_1^T\left(BP^{-1}B^T\right)^{-1}A_1 & A_1^T\left(BP^{-1}B^T\right)^{-1}A_2 \\ A_2^T\left(BP^{-1}B^T\right)^{-1}A_1 & A_2^T\left(BP^{-1}B^T\right)^{-1}A_2 + G^T P_c G \end{bmatrix} \begin{bmatrix} \hat{\delta}_1 \\ \hat{\delta}_2 \end{bmatrix} + \begin{bmatrix} A_1^T\left(BP^{-1}B^T\right)^{-1}w \\ A_2^T\left(BP^{-1}B^T\right)^{-1}w + G^T P_c w_c \end{bmatrix} = \begin{bmatrix} 0 \\ 0 \end{bmatrix} \quad (3)$$

where A_1, A_2 are the respective design matrices of partial derivatives of the functional (2) with respect to calibration and plane parameters, B is the design matrix of partial derivatives of the same functional taken with respect to the observations, G is the design matrix of partial derivatives of the linearized constrains imposed on the plane parameters, w is the misclosure vector, P and P_c are the weight matrices (often diagonal) related to observations and the constrain, respectively. The sparse structure of the design matrices allows formulating a contribution of individual observation equations in such a way that they can be added directly to the normal equations in a sequential manner. This enables the practical efficiency when using large LiDAR data sets.

3. AUTOMATED ROOF DETECTION

The described method for the parameter estimation was encoded into a program baptized LiBOR. The prerequisite for its correct functioning is the planarity of the selected surfaces. This assumption (i.e. no departures greater than the noise level of surface measurements) is indeed central to this method. Nevertheless, finding the planar features in the 'natural' terrain requires the use of sophisticated classification routines or visual guidance by means of orthophoto or approximate elevation models. Our experience in this regard has been that finding suitable natural terrain even on such 'planar' surfaces like soccer fields is problematic. On the other hand, their existence is relatively abundant within urban datasets. Moreover, surfaces like roofs often vary in aspect and slope, which is needed for good parameter de-correlation. The selection of rooftops can be performed by manual 'fence-drawing'; however, the classification needs to be done separately for each strip. Hence, there is a practical need to automate the roof selection process completely. Such automation should also minimize the existence of the outliers, i.e. points that do not belong to the surface (e.g. returns from antennas, chimneys, etc.).

The proposed algorithm follows the global workflow depicted in Fig. 1. First, the vegetation is removed and the roofs are identified within a reference strip (normally the strip with the best data quality) by means of a local covariance analysis, whose details will be described later. The location of the corresponding planes in the subsequent strips is approximately estimated by matching Digital Surface Models (DSM) derived from those strips with that of reference. The search is further refined for individual points by means of covariance analysis of the neighborhood and the surface boarders are finalized by region growing. The outcomes of this process are groups of points within different strips that can be conditioned to lie on a same plane. The individual steps of this process will be presented in more detail.

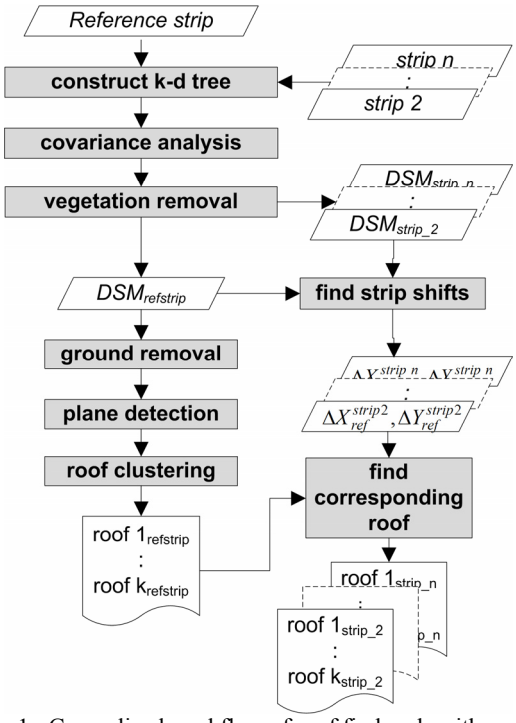

Figure 1: Generalized workflow of roof finder algorithm

3.1 Covariance analysis

The principle of local neighborhood covariance analysis is a key component for classifying the laser point cloud (Fig. 2). The estimate of a local covariance for a query point needs to be preceded by spatial indexing. This is achieved once for all points by the method of k-d tree decomposition. Local covariances are then computed for a pre-selected volume and their principle orientation is found by eigenvalue decomposition. It was previously reported that such approach is computationally very efficient mean of estimating surface normal vectors and local curvatures directly out of unstructured laser data (Bae and Lichti, 2004; Pauly et al., 2002).

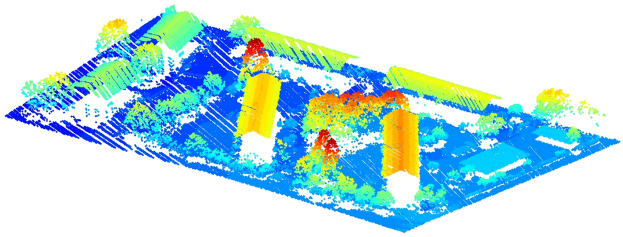

Figure 2: ALS point cloud of urban area with buildings and trees (color-coded by absolute height)

3.2 Roof detection within a strip

Referring to the algorithm flow in Fig. 1 the first step after the covariance analysis consists in the removal of points reflected by vegetation. In general, points belonging to the ground or buildings can be characterized by low curvature values (surface can often be approximated by a plane), whilst scanning points within vegetation and on roof edges generate high curvature values. These properties allow setting up a Boolean test based

on a threshold on the local curvature computed out of the local terrain normal (Schaer et al., 2007). The results of this selection are shown in Fig. 3 where points belonging to the trees and some points on the roof edges are identified in green.

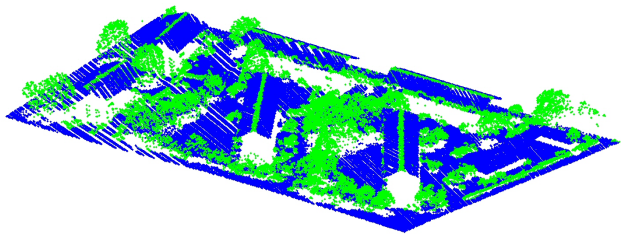

Figure 3: Removal of vegetation (mainly) by setting a threshold on local curvature estimate (in green)

The next step consists in removing all points belonging to the ground. By specifying a maximum building size and minimum building height for the area of interest, the algorithm searches for initial ground points (defined as the lowest point within a given cell, where cell size is larger than maximum building size). These points are used as initial query points to search for other point belonging to the ground until all points are classified (Fig. 4).

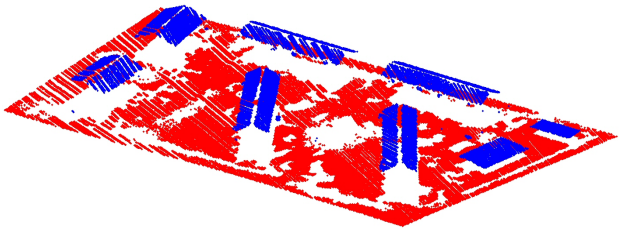

Figure 4: Removal of ground points (in red)

Once the points on the ground are identified, the remaining points can be clustered to points belonging to the same plane (thus to the same roof). This is achieved by a region growing approach that compares the estimated local terrain normals. In other words, two points ($\mathbf{p}_q$ and $\mathbf{p}_j$) are considered as belonging to the same plane when the following criteria are met (Fig. 5):

$$\text{on\_same\_plane}(\mathbf{p}_q,\mathbf{p}_j) = \begin{cases} TRUE \text{ if } \text{and}(\alpha_j^q \le atol, d_j^q \le dtol) \\ FALSE \text{ if } \text{or}(\alpha_j^q > atol, d_j^q > dtol) \end{cases} \quad (4)$$

Where

$$\mathbf{r}_j^q = \mathbf{p}_q - \mathbf{p}_j,\ d_j^q = \left\| \mathbf{r}_j^q \cdot \mathbf{n}_q \right\|,\ \alpha_j^q = \text{acos}\left(\frac{\mathbf{n}_j \cdot \mathbf{n}_q}{|\mathbf{n}_j||\mathbf{n}_q|} \right)$$

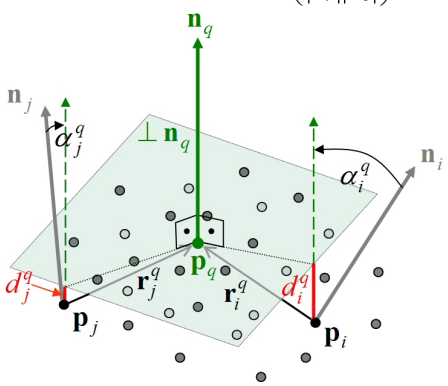

Figure 5: Comparison of local normal to evaluate if two points belong to the same plane

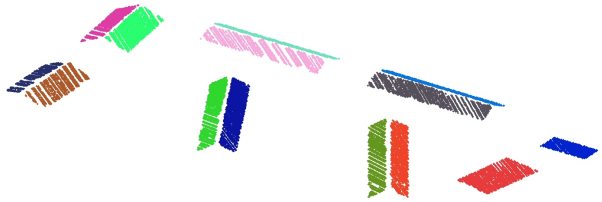

Figure 6: Points clustered to roof groups

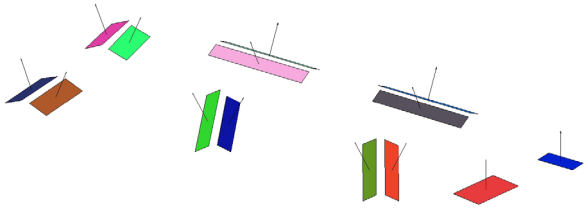

Figure 7: Computation of best fitting planes

Fig. 6 shows the result of the roof clustering step. Roof groups having fewer points than a certain threshold are removed automatically (minimal number of points for one group is defined by specifying minimal roof size). In the last step, the plane parameters for each roof are computed by the least square matching (Fig. 7).

3.3 Roof correspondence between strips

Prior to calibration, the initial boresight value is often considered as zero. Consequently, strip mismatches on the ground coordinates can reach several meters, even for boresight approximation better than a degree. Due to the possible existence of such large separation (mainly between flight lines of different orientation and altitude) the process of identifying the corresponding rooftops between strips is separated in two steps. An approximate 'global' shift between the strips is estimated first, and the search is refined in the second phase. The former employs the well known technique of raster matching by cross-correlation. Comparing the DSM of one strip to that of the reference strip yields a planar shift (ΔX, ΔY) that is applied as an approximate match.

Once the roof groups have been determined for the reference strip and the initial planar shifts have been applied, the search for a corresponding group is initiated from the reference group centre by applying the rules stipulated in Equation 4 and the area is augmented by regional growing.

3.4 Roof finder interface

To interactively control the results of the roof finder algorithm and eventually apply corrections (if necessary), the computations are guided by a Graphical User Interface (GUI). Within the GUI the user can easily adapt the processing parameters and visualize every intermediate result of the process. The interface also indicates the quality of the detected features in terms of standard deviation and maximum out-of-plane deviation (Figure 8).

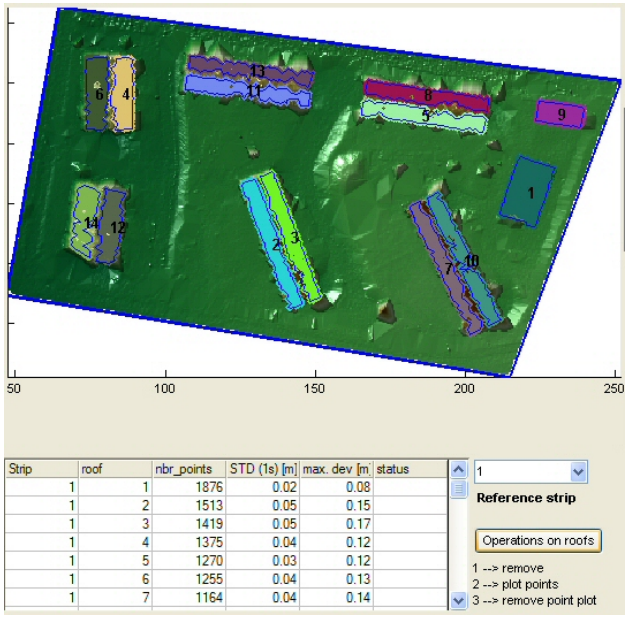

Figure 8: User interface of software for roof detection: the boundaries and the selected points for every roof are directly visualized on top of the DSM (vegetation already removed)

4. CALIBRATION EXAMPLES

In the following we present a synthesis of our experience when applying the presented adjustment methodology and automated roof-detection algorithm on data lasers of different scanning principles and from the market-leading manufactures like Optech, Leica and Riegl.

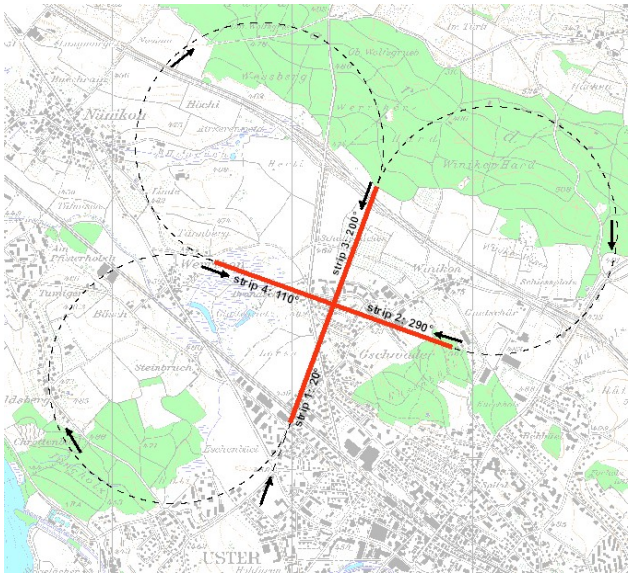

Figure 9: Typical calibration field and flight pattern

4.1 Calibration field(s) and flight pattern

The prerequisite for the choice of the calibration field selection is the presence of larger planar features (e.g. rooftops) that vary in aspect and inclination. This is typically the case of an urban area, as shown in Fig. 9. The same figure illustrates a cloverleaf flight pattern that is usually executed at two different altitudes. The variation of flight orientation and height is important for achieving good de-correlation between the estimated parameters.

4.2 Optech

The first example concerns the calibration of the Optech's ALTM 3100 airborne laser scanner. Its scanning principle employs an oscillating mirror that produces the zig-zag scanning pattern. The system operates at selected frequencies with maximum of 100 kHz, while about 75 kHz were used for the calibration. The maximum aperture is 50 degrees. To reduce some undesirable distortions due to imperfect design, this aperture is often limited to 22 degrees, as was the case for the calibration. The laser pulses have an aperture of 0.3mrad (e.g. this represents a laser dot size of 30cm at 1km distance) and the system allows to register up to four returns per single pulse. They are habitually equipped with Applanix 510 navigation system, which in this particular case consists of the LTN200-A1 IMU (1deg/h FOG) and Novatel L1/L2 GPS receiver. The flight pattern was executed twice as shown in Fig. 9, at 550 m and 1100 m above the ground.

Laser returns from 20 planes were selected to participate in the LiBOR adjustment. Some of these were used as “check planes”, i.e. planes that do not contribute to parameter estimation but are useful for control purposes. This is depicted in Fig. 10, on the out-of-plane residuals (1σ and maximum) plotted for previous and following adjustments.

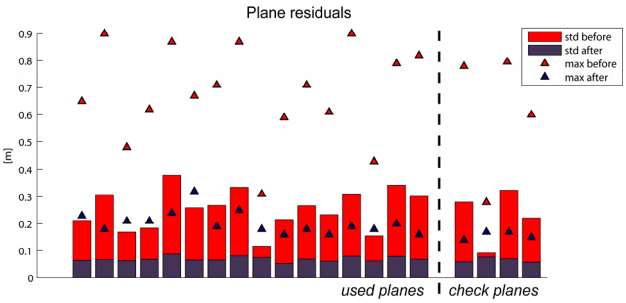

Figure 10: Out-of-plane residuals before and after adjustment (automated plane selection)

The groups of points per plane were first selected manually by drawing polygon lines separately for each strip. Second selection was made automatically by the proposed procedure. The results of boresight estimates for these two inputs are compared in Table 1. As it can be seen from this table the boresight values are practically the same for both selections, albeit the latter saved considerably the operator’s time.

Method	roll	Pitch	yaw	σ_r	σ_p	σ_y
	[deg]			[deg 10^{-3}]		
Manual	0.058	-0.031	0.038	0.2	0.2	2.5
Auto	0.058	-0.031	0.031	0.1	0.1	2.0
Optech	-0.054	-0.035	0.000	?	?	?

Table 1: Comparison of boresight estimates for Optech’s ALS

The boresight values are also compared to the best estimate provided by Optech for the same system. Optech’s boresight calibration strategy for this particular system employed the cross-section method that can relatively well estimate the boresight in roll and pitch, but is inappropriate for estimating the yaw angle. Therefore, there is a good agreement to those estimated by LiBOR in the roll and pitch angle, but there is a

large difference in yaw as the boresight in this direction was not estimated by the manufacturer.

4.3 Leica

Leica's ALS50 employs also an oscillating mirror and therefore has a similar scanning pattern to that of ALTM3100. The maximum scanning frequency and aperture are 150 kHz and 75 degrees, respectively. The laser pulses have an aperture of 0.33 mrad (e.g. this represents a laser dot size of 33cm at 1km distance). The type of navigation equipment varies with the year of fabrication. The calibration field was again in an urban area and flight pattern was similar to that of Fig. 9 but at altitude levels of 1000 m and 1500 m above the terrain. The combination of the flight speed, altitude and scanning frequency resulted in point densities of 2.6 pts/m^2 and 1.4 pts/m^2, respectively.

The choice of the flight parameters was not optimized for the LiBOR approach where more favorable geometry could be attained at lower flying height. This was due to a compromise with the calibration requirements according to a different methodology (Morin, 2002) that was performed simultaneously by the system owner. Nevertheless, this offers a possibility to compare the results attained by both calibration methods. As shown in Table 2, the differences are practically insignificant in roll and pitch but somewhat consequential in yaw. Nevertheless, the most outstanding discrepancy concerns the range finder offset, the value of which was assumed as calibrated (in well controlled environment of many GCPs). This effect should be, however, considered cautiously as ALS50 defines biases in range measurements separately for each of 255 possible intensity values. Although it can be assumed that the intensity values vary only little for the rooftops of similar kind, no detailed analysis has been performed in this respect. Nonetheless, the correlation of the range finder offset with the rest of the estimated parameters is investigated in the plot of Fig. 11. There it can be seen that it is not significantly correlated to other estimated parameters, and its value should therefore be considered as significant. Its relation to residual influences of other systematic corrections applied prior to LIBOR input then cannot be ruled out.

Method	roll	pitch	yaw	σ_r	σ_p	σ_v	$\Delta\rho$	$\sigma_{\Delta\rho}$
	[deg]			[deg 10^{-3}]			[cm]	
Libor	1.091	-0.645	0.024	.1	.1	.1	-23	1.2
Leica	1.091	-0.651	0.043	?	?	?	0	?

Table 2: Comparison of boresight estimates for Leica's ALS50

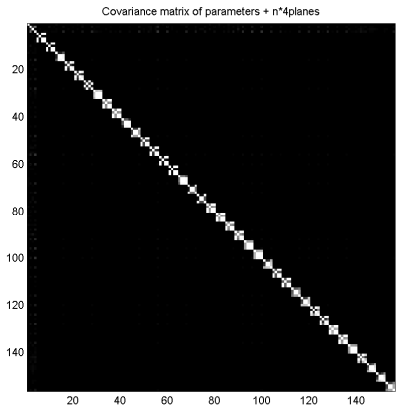

Figure 11: Correlation matrix between parameters where black=0 and white=1. The order of parameters is 3 boresight angles, $\Delta\rho$ followed by 4x47 plane coefficients

4.4 Riegl

The last presented examples concern the short-range 2D scanners (Riegl LMS Q240-x) with a scanning angle of 60° and maximum ranges of 450 (Q240) and 650 m (Q240i) at 80% reflectance. Its scanning mechanism employs rotating mirror providing unidirectional and parallel scanning pattern. The rate is chosen as a function of desired point density and flight parameters, typically several points per m^2 when transported by a helicopter. As the system is available to our research institute the results of calibrations are available for different IMU configuration as shown in Table 3.

LiDAR / IMU	roll	pitch	yaw	σ_r	σ_p	σ_v
	[deg]			[deg^{-3}]		
Q240/LN200	0.139	-0.060	-0.057	.7	.9	9.3
Q240i/FSAS	0.445	0.150	0.025	.7	.7	4.0

Table 3: Boresight estimates for different system configurations

Using a helicopter to carry the system allows reducing the flying height above the terrain, which has a favourable effect on the geometry (i.e. the inclination of the planes is larger across the swath). To some extent, the quality of the modelling can be judged from the distribution of observation residuals after the adjustment. Fig. 12 shows a histogram of the residuals for all 8-types of measurements together with their respective RMS. It can be noticed that all histograms are centred on zero (i.e. they are unbiased) and their respective RMS values are fairly small (i.e. mm or cm level in position and range; arc-second level for the angular quantities). The number of residuals close to zero is also reduced, which means that the geometry is such that most of the planes contribute to the estimates. Overall, it can be concluded that no important parameters were omitted from the model, and that the overall estimation is in good condition.

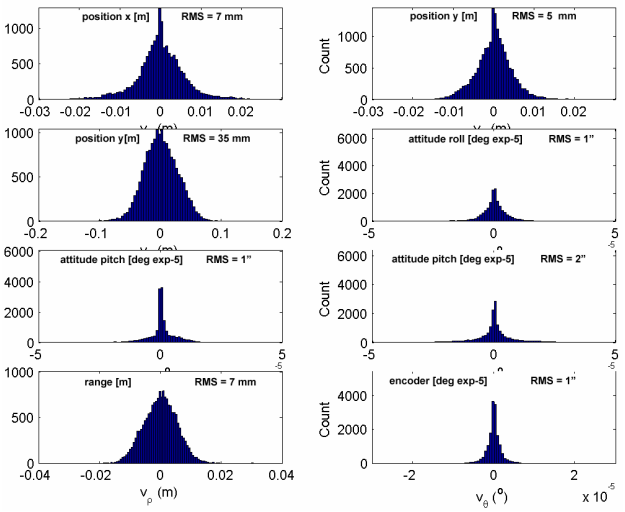

Fig. 12: Histogram of measurement residuals for the urban data of strong geometry

5. CONCLUSIONS

The 'LiBOR' approach on boresight self-calibration in airborne laser scanning was studied in light of its practicability. After recalling its underlying adjustment principles the emphasis was given on the automation of its input, i.e. separation and classification of planar rooftops segment per plane and strip.

The experience confirms the suitability of the presented algorithm for urban areas where the buildings are separated and have relatively simple roof structure (e.g. as in Fig. 2). For a situation where the 'roof landscape' is complex (e.g. buildings are attached in varying angles or large presence of dormer windows, chimneys, etc.) the algorithm has more difficulties to locate suitable planar features. In such a case small assistance can be easily applied via the roof finder GUI by specifying a polygon around roof borders by means of visual guidance based on the DSM of the reference strip. On the other hand, the selection of the appropriate points and the search of rooftops correspondences in other strips remain completely autonomous. The practical examples were given for instruments from three market leaders in the ALS industry. In all cases the comparison of parameter mean values and accuracy estimated by LiBOR was either equal or superior to that based on the methods proposed by its manufactures. Hence, the benefits of the studied method are not only in the rigorous modeling and automation but also in its suitability to systems of different providers or scanning principles.

6. ACKNOWLEDGMENT

This work was mostly funded by the Swiss Commission for Innovation (CTI/KTI Project 7782 EPRP) in collaboration with Swissphoto AG. The authors thank greatly to Derek Lichti for his help in k-d tree implementation and advices on covariance analyses.

REFERENCES

Bae, K.-H. and Lichti, D., 2004. Edge and Tree Detection from Three-dimensional Unorganised Point Clouds from Terrestrial Laser Scanners, 12th Australian Remote Sensing and Photogrammetry Conference, Fremantle, Australia

Burman, H., 2000. Calibration and orientation of airborneiImage and laser scanner data using GPS and INS, Royal Institute of Technology, Stockholm, 107 pp

Cramer, M. and Stallmann, D., 2002. System Calibration For Direct Georeferencing, Photogrammetric Computer Vision, ISPRS Commission III Symposium, Graz, Austria, pp. 6. http://www.isprs.org/commission3/proceedings/

Filin, S., 2003. Recovery of Systematic Biases in Laser Altimetry Data Using Natural Surfaces. Photogrammetric Engineering and Remote Sensing, 69(11): 1235-1242

Friess, P., 2006. Toward a rigorous methodology for airborne laser mapping., EuroCOW. on CDROM, Castelldefels, Spain, pp. 7

Kruck, E., 2001. Combined IMU and sensor calibration with BINGO-F, Integrated Sensor Orientation, Proc. of the OEEPE Workshop ". CD-ROM, Hannover, pp. 84-108

Morin, K., 2002. Calibration of airborne laser scanners, The University of Calgary, 135 pp.

Pauly, M., Gross, M. and Kobbelt, L.P., 2002. Efficient simplification of point-sampled surfaces, IEEE Conference on Visualization, Boston

Schaer, P., Skaloud, J., Landtwing, S. and Legat, K., 2007. Accuracy Estimation for Laser Point Cloud including Scanning Geometry, 5th International Symposium on Mobile Mapping Technology (MMT2007), Padua, Italy

Schenk, T., 2001. Modeling and Analyzing Systematic Errors in Airborne Laser Scanners. In: C.a.E.E.a.G. Science (Editor). The Ohio State University

Skaloud, J. and Lichti, D., 2006. Rigorous approach to bore-sight self calibration in airborne laser scanning. ISPRS Journal of Photogrammetry and Remote Sensing, 61: 47-59

Skaloud, J. and Schaer, P., 2003. Towards A More Rigorous Boresight Calibration, ISPRS International Workshop on Theory Technology and Realities of Inertial/GPS/Sensor Orientation, Castelldefels, Spain